Supplementary Information 1: Opacity from particle positions

In this supplementary information section we provide the conversion between the cell output positions obtained by microscopic observation and the opacity values related to the dielectric properties of the yeast cells. These positions arise through the focusing action of the dielectrophoretic force field in the active element, followed by a fluidic redistribution due to a channel enlargement necessary for convenient observation (Supplementary Fig. 1), so that reconstruction of the dielectric opacity values from the output particle stream position requires both a fluidic mapping and the opacity reconstruction per se. In this Supplementary Information, section 1 deals with the opacity reconstruction, whereas section 2 addresses the fluidic mapping aspect.

1 Particle Equilibrium Positions and Opacity Reconstruction

We have shown that the final equilibrium position in our sorting channel is a function of ratio of the forces acting on the cells from the two sides, and that vice versa, observation of the equilibrium positions allows to estimate this force ratio[1]:

$$\frac{< F_1(0) >}{< F_2(0) >} = g(y_{eq}) \tag{1}$$

where the notation $F_1(0)$ and $F_2(0)$ indicates that the force ratio is measured at the channel midline, at the equilibrium position it would be always equal to 1 by definition. The function $g(y_{eq})$ results from the electric field geometry, we shall discuss it below.

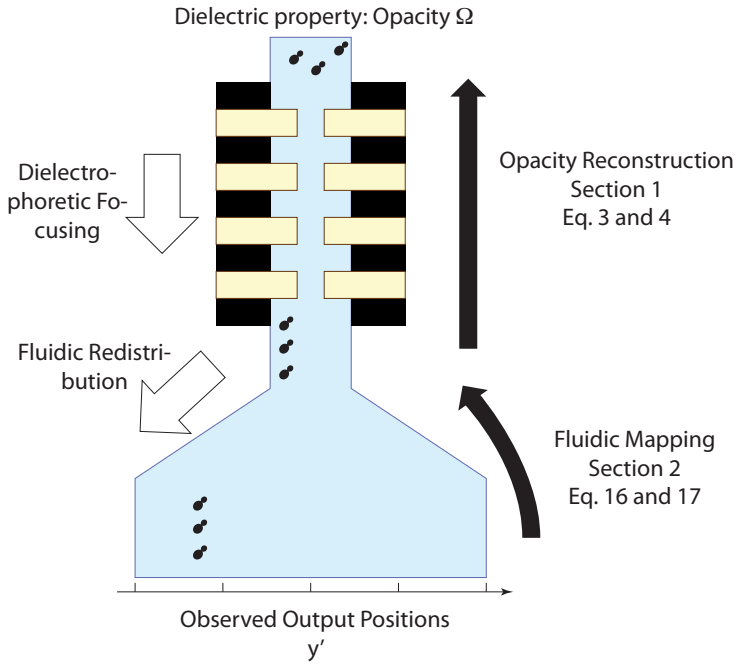

Supplementary Figure 1: Origin of the cell positions and mapping procedure. The cell positions result from a double process. Firstly, the dielectrophoretic forces focus each particle type to its characteristic flow line. This position is a function of the applied voltages and frequencies, and of the intrinsic particle properties, in particular the opacity Ω. Second, we use a channel enlargement after the electrically active element to slow down the flow and ease observation. This implies fluidic redistribution, which we need to take into account when reconstructing the opacity values from the output particle positions. The overall mapping procedure for the retrieval of the opacity is indicated on the right hand side of the figure.

In a typical setting, we focus the cells towards the channel midline using repulsive dielectrophoretic forces acting from both sides of the channel, using a low frequency signal on each side ($V_{lf,1}$ and $V_{lf,2}$). To induce the cell sorting, we add a high frequency signal on one side (V_{hf} superimposed on $V_{lf,1}$). The resulting force ratio, as measured at the channel midline is:

$$\frac{F_1}{F_2} = \frac{V_{lf,1}^2 + \frac{\Re f_{\mathrm{CM}}(hf)}{\Re f_{\mathrm{CM}}(lf)} \cdot V_{hf}^2}{V_{lf,2}^2} = \frac{V_{lf,1}^2 + \Omega \cdot V_{hf}^2}{V_{lf,2}^2} \tag{2}$$

where the opacity is as defined as the ratio of the real parts of f_{CM} at the frequencies involved (cf. eq. 2 in the main text).

Combining eq. 2 and eq. 1, we see that the opacity can be estimated from the equilibrium positions according to:

$$\Omega = \frac{g(y_{eq})V_{lf,2}^2 - V_{lf,1}^2}{V_{hf}^2} \tag{3}$$

In the past, we have used conformal mapping to obtain the electric field distribution and hence $g(y_{eq})$[1]. While there is good agreement between predicted and observed particle positions in calibration experiments with isolating polystyrene microbeads[1], the formulas involved are rather complicated and require mathematical software such as Matlab for their evaluation.

It has been pointed out[2] that the dielectrophoretic force field of an interdigitated electrode array can be approximated by an exponentially decaying function, the approximation being better

at greater distance from the array. Even though in our channel geometry the electric field is forced into the horizontal plane rather than being able to spread out vertically, our arrangement of alternatingly powered electrodes along the sorting channel still strongly resembles an interdigitated electrode array.

Supplementary Figure 2 shows that it is possible to approximate the $g(y_{eq})$ function as obtained from the conformal mapping approach by an exponential, with very good agreement in the central region of the channel. We can therefore approximate $g(y_{eq})$ by:

$$g(y_{eq}) \approx e^{\alpha \frac{y_{eq}}{w}} \tag{4}$$

where the coefficient α can be obtained by equalizing the slopes for $y_{eq} = 0$, it has a value of $\alpha \approx 6.5$.

This is close to $\alpha = 2\pi$, expected on theoretical grounds using the result presented in [2]. Indeed according to [2], the dielectrophoretic force produced by an interdigitated electrode array decays with a constant of $\frac{\pi}{w}$, but since we oppose two forces, one increasing and the other decreasing when going away from the channel midline, we expect a decay constant of $\frac{2\pi}{w}$, and hence $\alpha = 2\pi$.

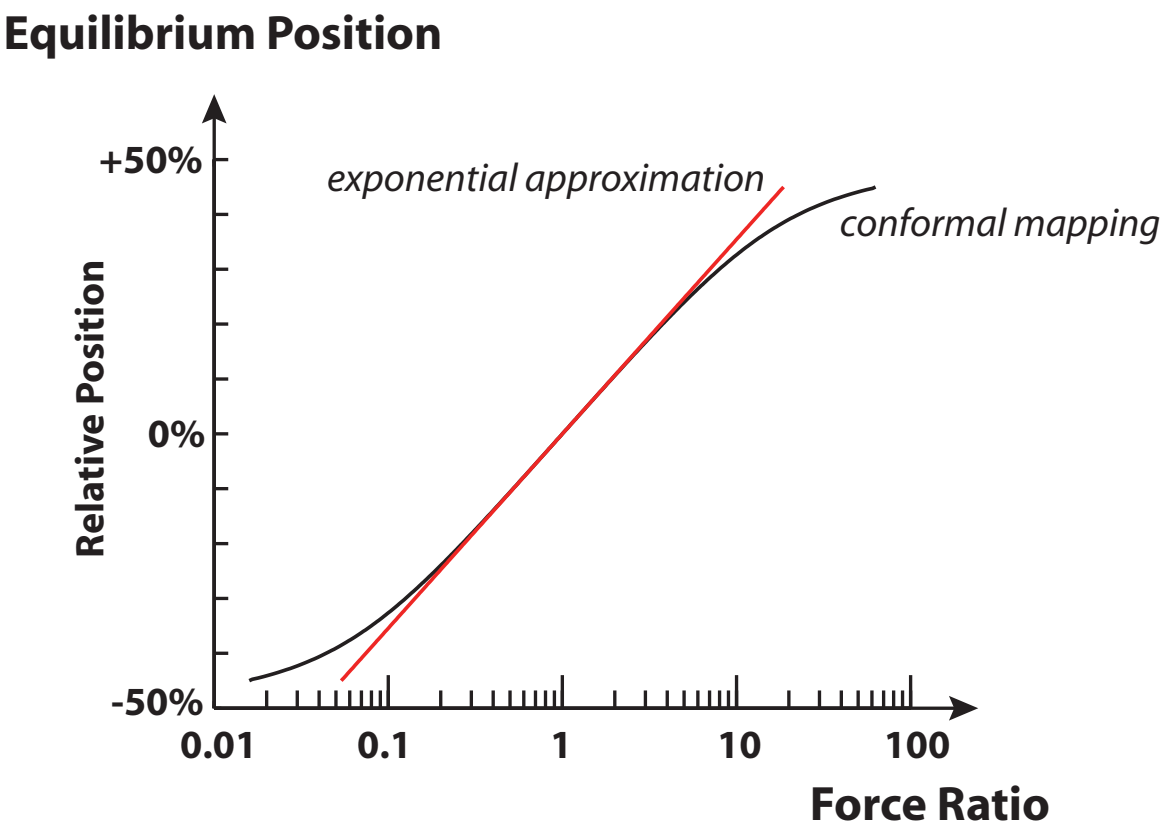

Supplementary Figure 2: Relation between the force ratio and the particle equilibrium position. The equilibrium position of the particles is determined by the ratio of the forces acting from the two electrode arrays; inversely, the force ratio and hence the dielectric properties can be inferred from the lateral position of the focused particle stream. The figure shows the particle positions as a function of the force ratio. The curve labelled "conformal mapping" is obtained from the electrical field as estimated by the conformal mapping technique [3], whereas the curve labelled "exponential approximation" is obtained semi-empirically as by fitting an exponential of the form (force ratio) = $e^{\alpha y_{eq}}$ to the central part of the relation obtained by conformal mapping.

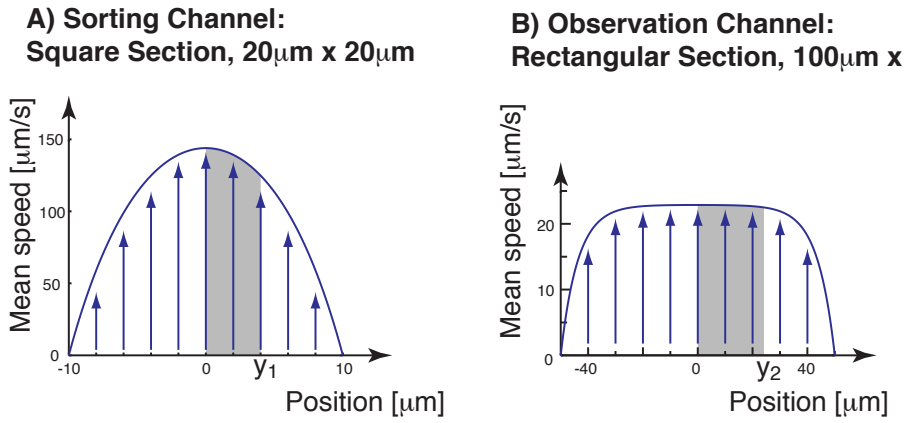

Supplementary Figure 3: Conservation of mass leads to redistribution of the flow lines. The quadrangular section of the sorting channel leads to a near parabolic distribution of the velocity across the channel, as shown in Supplementary Figure 3-A. In the observation region, the low aspect ratio ($h \ll w$) leads to a more flat velocity profile along the horizontal direction (Supplementary Fig. 3-B). The conservation of mass implies that the amount of fluid transported between the channel midline, which is the symmetry axis of the channel, and homologous positions must be equal. In mathematical terms, if y_1 and y_2 are corresponding flow lines in the two channel sections, the integrals from 0 to y_1 and 0 to y_2, shown as grey areas in the figure, are equal.

2 Fluidic Mapping

The dielectric properties of the yeast cells, together with the applied voltages and frequencies, determine the equilibrium positions in the sorting channel. However, following the sorting channel, we have a large observation channel, and the channel cross-section passes from 20μm x 20μm to typically 100-300μm x 20μm. While of great practical advantage due to the slowdown of the liquid for fluorescence observation, this induces a fluidic redistribution. Indeed, in a square section, the laminar flow profile implies a nearly parabolic flow profile both horizontally and vertically across the channel, whereas in a horizontal wide channel, the flow profile is parabolic only along the vertical direction, but more nearly flat along the horizontal direction. Conservation of mass then implies redistribution of the flow lines, as shown in Supplementary Figure 3. In order to correctly evaluate the particle opacities, we need to correct for this effect. We shall now derive simple formulas for the mapping between the positions in the sorting channel of square section and the wide rectangular observation channel.

We use a 2D approximation to obtain the evolution of the particle positions when the channel cross section changes. In a channel with laminar flow, conservation of mass implies that corresponding segments of the fluid flow must transport the same amount of fluids at all cross sections of the channel. This means that the grey areas, shown in Supplementary Figure 3, representing the fluid flow transport, must be identical if y_1 and y_2 represent corresponding flow lines at the two sections of the channel shown. Supposing that the channel height remains constant, we have:

$$\left(\frac{\mathrm{d}Q}{\mathrm{d}t}\right)_{y_1} = \int_0^{y_1} v_1(y)(d)y = \left(\frac{\mathrm{d}Q}{\mathrm{d}t}\right)_{y_2} = \int_0^{y_2} v_2(y')(d)y' \tag{5}$$

The local velocity in rectangular channel cross section of height h and width w is given by[4,5]:

$$v_{\text{fluid}}(y,z) = \frac{4h^2\Delta P}{\pi^3\eta L} \cdot \sum_{n,\,\text{odd}}^{\infty} \frac{(-1)^{\frac{n-1}{2}}}{n^3} \left[1 - \frac{\cosh\left(n\pi\frac{y}{h}\right)}{\cosh\left(n\pi\frac{w}{2h}\right)}\right] \cos\left(n\pi\frac{z}{h}\right) \tag{6}$$

P being the pressure, η the dynamic viscosity and L length of the channel; by using the $\cos$ terms, the coordinate system is centred on the channel center, y spanning the width the channel, and z the height.

The mean velocity for a given position across the channel width is obtained by averaging along the z direction, using the relation $(-1)^{\frac{n-1}{2}} \cdot \sin\left(\frac{n\pi}{2}\right) = 1$ for n odd:

$$v_{\text{fluid}}(y) = \frac{1}{h} \cdot \int_{-\frac{h}{2}}^{\frac{h}{2}} v_{\text{fluid}}(y,z)\mathrm{d}z = \frac{8h^2\Delta P}{\pi^4\eta L} \cdot \sum_{n,\,\text{odd}}^{\infty} \frac{1}{n^4} \left[1 - \frac{\cosh\left(n\pi\frac{y}{h}\right)}{\cosh\left(n\pi\frac{w}{2h}\right)}\right] \tag{7}$$

The pressure drop per unit channel length, $\frac{\Delta P}{L}$, varies along the channel when the cross section changes whereas the total flow rate $\frac{\mathrm{d}Q_{\text{total}}}{\mathrm{d}t}$ does not. We therefore express the velocity distribution across the channel as a function of the total flow rate rather than of the pressure drop. To do so, we combine the expression for the total flow rate given in [5] with eq 7, we get:

$$v_{\text{fluid}}(y) = \frac{\mathrm{d}Q_{\text{total}}}{\mathrm{d}t} \cdot \frac{1}{hw} \cdot \frac{1 - \frac{96}{\pi^4} \sum_{n,\,\text{odd}}^{\infty} \frac{1}{n^4} \left[\frac{\cosh\left(n\pi \frac{y}{h}\right)}{\cosh\left(n\pi \frac{w}{2h}\right)} \right]}{1 - \frac{96}{\pi^5} \cdot \frac{2h}{w} \cdot \sum_{n,\,\text{odd}}^{\infty} \frac{1}{n^5} \tanh\left(n\pi \frac{w}{2h}\right)} \tag{8}$$

where we have used $\sum_{n,\,\text{odd}}^{\infty} \frac{1}{n^4} = \frac{\pi^4}{96}$ from [5].

In the sorting channel, the flow profile is nearly parabolic and we can approximate eq. 8 by the parabolic flow profile of an infinite plate geometry, given by[5]:

$$v_1(y) = \frac{\mathrm{d}Q_{\text{total}}}{\mathrm{d}t} \cdot \frac{1}{h^2} \cdot \left[\frac{3}{2} - \frac{6y^2}{h^2} \right] \tag{9}$$

In the observation channel, we can approximate the flow speed as being constant and equal to maximum flow speed v_{max} predicted in the center of the channel, but over a reduced apparent channel width w_{eff}:

$$v_2(y') = \begin{cases} v_{\text{max}} \text{ for } |y'| \leq \frac{w_{\text{eff}}}{2} \\ 0 \text{ otherwise} \end{cases} \tag{10}$$

We estimate v_{max} using eq. 8 for $y = 0$:

$$v_{\text{max}} = v_{\text{fluid}}(0) = \frac{\mathrm{d}Q_{\text{total}}}{\mathrm{d}t} \cdot \frac{1}{hw} \cdot \frac{1 - \frac{96}{\pi^4} \sum_{n,\,\text{odd}}^{\infty} \frac{1}{n^4} \cdot \frac{1}{\cosh\left(n\pi \frac{w}{2h}\right)}}{1 - \frac{96}{\pi^5} \cdot \frac{2h}{w} \cdot \sum_{n,\,\text{odd}}^{\infty} \frac{1}{n^5} \tanh\left(n\pi \frac{w}{2h}\right)} \tag{11}$$

For $w \gg h$, we can use $\cosh(x \gg 1) \gg 1$ and $\tanh(x \gg 1) \approx 1$ such that we get:

$$v_{\text{max}} \approx \frac{\mathrm{d}Q_{\text{total}}}{\mathrm{d}t} \cdot \frac{1}{hw} \cdot \frac{1}{1 - \frac{96}{\pi^5} \cdot \frac{2h}{w} \cdot \sum_{n,\,\text{odd}}^{\infty} \frac{1}{n^5}} \approx \frac{\mathrm{d}Q_{\text{total}}}{\mathrm{d}t} \cdot \frac{1}{h} \cdot \frac{1}{w - \frac{192}{\pi^5} \cdot h} \tag{12}$$

In order to estimate w_{eff} we use the conservation of the total volume flow rate:

$$hw_{\text{eff}} \cdot v_{\text{max}} = \frac{\mathrm{d}Q_{\text{total}}}{\mathrm{d}t} \tag{13}$$

so that we get for w_{eff}:

$$w_{\text{eff}} \approx w - \frac{192}{\pi^5} \cdot h = w - 0.63 \cdot h \tag{14}$$

Evaluation of the mass conservation equation (eq. 5) for the two flow profiles given by eq. 9 and eq. 10 yields a mapping from the square section to the wide channel section:

$$y' \;=\; \frac{y}{h} \cdot \left(\frac{3}{2} - 2 \left(\frac{y}{h} \right)^2 \right) \cdot w_{\text{eff}} \tag{15}$$

In practice, we observe y' in the observation channel and need estimate y in the sorting channel. Solving eq. 15 for y yields:

$$y = \sigma_y \cdot \frac{\cos\alpha_y - \sqrt{3}\cdot\sin\alpha_y}{2} \cdot h \tag{16}$$

where σ_y is the signum function of y', i.e. it is 1 if $y' \geq 0$ and -1 otherwise. α_y is defined by:

$$\alpha_y = \frac{1}{3} \cdot \tan^{-1}\left(\sqrt{\left(\frac{w_{\text{eff}}}{2y'}\right)^2 - 1}\right) \tag{17}$$

where $\tan^{-1}$ designates the functional inverse of the tangent, i.e. the arc tangent function. Eq. 17 requires that $|y'| \leq \frac{w_{\text{eff}}}{2}$, indicating that the flow lines in the wide channel spread only over the effective width and not the entire channel width, in agreement with the initial hypothesis of a flat velocity profile limited to an effective channel width given by w_{eff}. Further, for $y' = 0$, we get a division by zero in eq. 17, but we can use $\tan^{-1}(+\infty) = \frac{\pi}{2}$ so that $\alpha_y(y' = 0) = \frac{\pi}{6}$, and, using the special values of the $\sin$ and $\cos$ functions at $\frac{\pi}{6}$, we obtain $y = 0$ as it ought to be for the symmetry axis of the channel.

1. Demierre, N., Braschler, T., Muller, R. & Renaud, P. Focusing and continuous separation of cells in a microfluidic device using lateral dielectrophoresis. *Sensors And Actuators B-Chemical* **132**, 388–396 (2008).

2. Morgan, H., Izquierdo, A., Bakewell, D., Green, N. & Ramos, A. The dielectrophoretic and travelling wave forces generated by interdigitated electrode arrays: analytical solution using fourier series. *Journal Of Physics D-Applied Physics* **34**, 2708–2708 (2001).

3. Braschler, T. *Controlled Entrapment of Cells in Hydrogels on Chip and Cell Sorting by Dielectrophoresis using Liquid Electrodes*. Ph.D. thesis, Ecole Polytechnique Federal de Lausanne (2009).

4. Grizzuti, N., Guido, S., Nastri, V. & Marrucci, G. Velocity profiles in rectangular channel flow of liquid crystalline polymer solutions. *Rheologica Acta* **30**, 71–76 (1991).

5. Bruus, H. *Theoretical Microfluidics* (Oxford University Press, 2008).

Supplementary Information 2: Geometrical Life History for Budding Yeast

Geometric variables We model yeast cells as ellipsoids with cylindrical symmetry, that is, as ellipsoids having two equal half axes and a distinct, generally longer half axis along the symmetry axis (Supplementary Fig. 1-A). Single cells are modelled as single ellipsoids, dividing cells as connected ellipsoids sharing the rotational symmetry axis (Supplementary Fig. 1-B). The shape of a single ellipsoid with cylindrical symmetry can be described by its eccentricity, being defined as the ratio of the length of the half axis along the rotational symmetry axis as compared to the length of the half axis perpendicular to the symmetry axis (Supplementary Fig. 1-A). The evolution of the eccentricity with growing cell size is sufficient to characterize the growth history up to division, and after cytokinesis. For cells engaged in division, in addition, the ratio of the bud size as compared to the mother cell size is needed.

For reasons of convenience, we choose the visible cross-section area of the cells, in μm^2, in microscopic observations as a measure for cell size. For the observation of the long and short axis by conventional microscopy, it is necessary that the rotational symmetry axis is in the observation plane. Fortunately, the cells are usually prolate rather than oblate ellipsoids, and orient their long axis in the electric field, which is parallel to the observation plane in our device. Using the nomenclature given in Supplementary Fig. 1-B, the mother and bud areas can be calculated as $\pi \cdot a \cdot c$ and $\pi \cdot a_{\text{bud}} \cdot c_{\text{bud}}$ respectively.

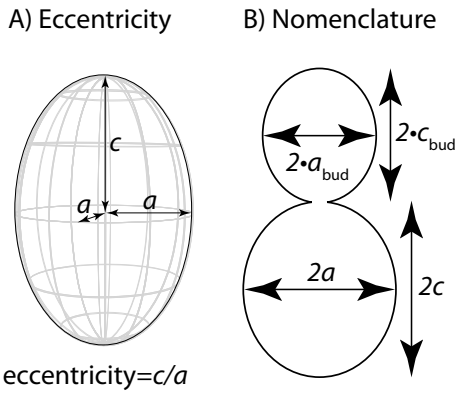

Supplementary Figure 1: Geometric Variables. A) For an ellipsoid with rotational symmetry, we define the eccentricity as being the ratio of the length of the half axis along the symmetry axis c as compared to the length of the half axis a perpendicular to it. B) Model of a budding yeast cell; mother cell and bud share a common rotational symmetry axis along c and c_{bud}.

Eccentricity The eccentricity varies in a characteristic way for yeast cells of different sizes, as shown in Supplementary Fig. 2-A. The eccentricity is typically close to 1 for very small cells, distinctly larger than 1 for intermediate stages, returning towards 1 for the largest cells. This is because the very small and very large cells are spherical, whereas medium size cells are elongated. We model this variation by a second order polynomial function, as shown by the best-fit line in Supplementary Fig. 2-A. We obtain a least-squares best fit as follows:

$$\text{eccentricity} = 0.969 + 0.01802\mu\text{m}^{-2} \cdot A - 0.0003666761\mu\text{m}^{-4} \cdot A^2 \qquad (1)$$

where A is the cross-sectional area of the cell. The eccentricity as calculated from eq. 1 is shown as red theoretical line in Supplementary Fig. 2-A. The underlying geometrical mea-

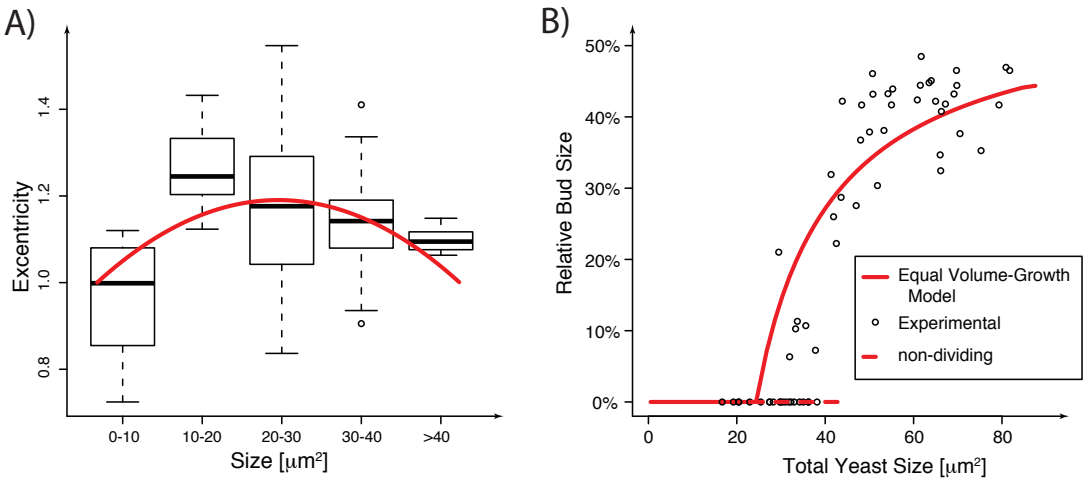

Supplementary Figure 2: Geometric parameters changes in yeast life history. A) Eccentricity as a function of cell size. We describe cell eccentricity as a second order polynomial function of the size as measured by the visible cross sectional area. B) Variation of yeast cell size during division quantified by the visible cross-section area of mother and daughter cells. The model is obtained under the assumption that cell division always occurs at a specific cell volume and that after cell separation, mother and daughter cells exhibit equal volume growth, leading to a non-linear relation of the visible cross-section area. The red curves are least square best-fits to the experimental data.

surements are obtained from a growing yeast culture, including pooled data from single cells and budding cells.

Mother and Daughter cell volume In a given population, a correlation between the total size of the cell doublets and the relative bud size can be observed (Supplementary Fig. 2-B). The variation in the bud-to-mother size ratio can be approximately explained by a model assuming that division occurs at a given critical cell volume and that after cell separation, mother and daughter cells experience a similar increase in volume; the eccentricity relation can be used to convert between the areas and the cell volume. We further assume no mass transfer between mother and daughter. This model is only approximative because the maximal volume cells can acquire is limited, and therefore the change in volume of large cells must decrease.

By least squares fitting, we find a critical division volume of

$$V_{\text{division}} = 83.4\mu\text{m}^3 \tag{2}$$

in agreement with flow cytometry measurements[1]. In terms of mother and daughter volumes, the equal volume growth model implies:

$$V_{\text{mother}} - V_{\text{bud}} = V_{\text{division}} \tag{3}$$

Neck size The finite neck size in principle leads to an overlap between the mother and daughter ellipsoids, making a full distinction between mother and daughter volume difficult. However, except for very small buds, the neck is relatively narrow (diameter of the cytoplasmic part approximately 500nm) , so that we neglect this overlap effect. Hence, for geometrical considerations, we model mother and daughter as full rather than cut ellipsoids.

Application example The equal volume growth model together with the evolution of the eccentricity is sufficient to obtain an approximate geometrical description of yeast cells throughout the division cycle. As a practical example, we shall obtain the typical mother and daughter half axis lengths for a visible mother area of A=35μm^2. According Eq. 1, we expect an eccentricity value of 1.15. Since the cross-sectional area of an ellipse is given by πac, a and c being the short respectively long half axis, we obtain $a = 3.11\mu$m, and $c = 3.58\mu$m for the mother. The mother volume is then obtained as the volume of the ellipsoid with cylindrical symmetry, given by $\frac{4\pi}{3}a^2c = 145.2\mu\text{m}^3$. The bud volume follows from eq. 3: $V_{\text{bud}} = 61.8\mu\text{m}^3$. In order to find the half axes lengths a_{bud} and c_{bud} we need to solve the following equation system:

$$\begin{cases} \frac{c_{\text{bud}}}{a_{\text{bud}}} = 0.969 + 0.01802\mu\text{m}^{-2} \cdot \pi a_{\text{bud}} c_{\text{bud}} - 0.0003666761\mu\text{m}^{-4} \cdot \pi^2 a_{\text{bud}}^2 c_{\text{bud}}^2 \\ 61.8\mu\text{m}^3 = \frac{4\pi}{3} a_{\text{bud}}^2 c_{\text{bud}} \end{cases} \tag{4}$$

Solving eq. 4 numerically yields $a_{\text{bud}} = 2.32\mu$m and $c_{\text{bud}} = 2.74\mu$m and hence a bud eccentricity of $\frac{2.74\mu\text{m}}{2.32\mu\text{m}} = 1.18$.

1. Tamaki, H. *et al.* Glucose-dependent cell size is regulated by a g protein-coupled receptor system in yeast saccharomyces cerevisiae. *Genes To Cells* **10**, 193–206 (2005).

Supplementary information 3: Estimation of the equivalent permittivity of dividing yeast cells

This supplementary information details how the equivalent permittivities of single and dividing yeast cells can be calculated.

1 Problem Statement

The dielectrophoretic force on a particle of arbitrary shape depends on the Clausius-Mossotti factor, which is given by equation 3 in the main text:

$$f_{\mathrm{CM}}(\omega) = \frac{\epsilon_p^*(\omega) - \epsilon_m^*(\omega)}{\epsilon_m^*(\omega) + \left[\epsilon_p^*(\omega) - \epsilon_m^*(\omega)\right] \cdot n_x} \tag{1}$$

This Supplementary Information details how the complex permittivity of the particle ϵ_p^* at a given angular frequency ω can be obtained. The calculation of the form factor n_x, depending only on the particle geometry, can be found in Supplementary Information 4.

2 Material Properties

In terms of electrical properties, we consider three distinct regions: the suspension medium (with permittivity ϵ_m and conductivity σ_m), the cytoplasm (with permittivity ϵ_{cyto} and conductivity σ_{cyto})

and cell membrane (with permittivity ϵ_{mem} and conductivity σ_{mem}). For each of these regions, the frequency-dependent complex permittivity is defined by the generic relation $\epsilon^* = \epsilon + \frac{\sigma}{i\omega}$. We do not explicitly simulate the cell wall, since its conductivity and permittivity are close to the values of the extracellular medium[1] when the medium conductivity is not very low, such that the presence of the wall should only have minor influence on the dielectrophoresis of budding yeast. The numerical values used are summarized in table 1; they are taken from [2], with the exception of the conductivity of the suspension medium, which we measure. The electric properties of the suspension medium are needed to evaluate $\epsilon_m^* = \epsilon_m + \frac{\sigma_m}{i\omega}$ in eq. 1, the other properties are needed to evaluate ϵ_p^*.

3 Single Cells

We model the single cells as rotationally symmetrical prolate ellipsoids, with a long axis along the electric field and the two short axes perpendicular to it. The ratio of long to short axis is termed eccentricity; Supplementary Information 2 describes the evolution of the eccentricity for different cell sizes.

A multi-shell model suitable for biological cells of ellipsoidal shape is available in literature[3,4]; this model takes in particular into account that the membrane has a constant thickness, implying that the inner and outer membrane surface are in fact not confocal ellipsoids.

According to this model, the equivalent permittivity of a generic particle with core-shell structure is:

Quantity	Value
Cytoplasm conductivity σ_{cyto}	300 mS/m
Cytoplasm permittivity ϵ_{cyto}	$50 \cdot \epsilon_0$
Membrane conductivity σ_{mem}	0.25 μS/m
Membrane permittivity ϵ_{mem}	$6 \cdot \epsilon_0$
Medium conductivity σ_m	60 mS/m
Medium permittivity ϵ_m	$78 \cdot \epsilon_0$
Membrane thickness d	8 nm
Cell geometry (a, c for single cells)	cf. Supplementary Information 2
Cell geometry (a, c, a_{bud}, c_{bud} for dividing cells)	cf. Supplementary Information 2
Neck diameter s	Best fit $s = 0.4 \cdot a_{\text{bud}}$, $s \to 0$ in cytokinesis

Table 1: Material constants and dimensions used for the finite element simulation of the dividing yeast cells. ϵ_0 is the vacuum permittivity, given by $\epsilon_0 = 8.85\frac{C}{Vm}$. The values for σ_{cyto}, ϵ_{cyto}, σ_{mem}, ϵ_{mem} and d are taken from [2]; σ_m is measured using a conductivity-meter, while the medium permittivity ϵ_m is assumed to be equal to the one of water.

$$\epsilon_p^* = \epsilon_{\text{shell}}^* \cdot \frac{1 + 3(1 - n_x) \cdot \phi_{\text{core}} \cdot f_i}{1 - 3n_x \cdot \phi_{\text{core}} \cdot f_i} \tag{2}$$

where n_x is the form factor, and ϕ_{core} is the volume fraction occupied by the core. f_i is an inner Clausius-Mossotti factor, reflecting the combined contribution of core and shell:

$$f_i = \frac{1}{3} \cdot \frac{\epsilon_{\text{core}}^* - \epsilon_{\text{shell}}^*}{\epsilon_{\text{shell}}^* + n_x \cdot (\epsilon_{\text{core}}^* - \epsilon_{\text{shell}}^*)} \tag{3}$$

The form factor n_x, also referred to as Lorentz depolarisation factor, is well known for ellipsoids. For the prolate ellipsoids used here it is given by[5]:

$$n_x = \frac{1}{1 - \left(\frac{c}{a}\right)^2} - \frac{c}{a} \cdot \frac{\ln\left(\frac{c}{a} - \sqrt{\left(\frac{c}{a}\right)^2 - 1}\right)}{\left[\left(\frac{c}{a}\right)^2 - 1\right]^{\frac{3}{2}}} \tag{4}$$

where the electric field vector is along $c > a$. For spherical particles, $n_x = \frac{1}{3}$.

The core-shell model given by eq. 2 is designed to be used recursively for multi-layered cell structures. However, since we neglect the cell wall, there is no need to do so, and the equivalent permittivity ϵ_p^* can be obtained directly from eq. 2 and 3 by setting $\epsilon_{\text{shell}}^* = \epsilon_{\text{mem}}^* = \epsilon_{\text{mem}} + \frac{\sigma_{\text{mem}}}{i\omega}$ and $\epsilon_{\text{core}}^* = \epsilon_{\text{cyto}}^* = \epsilon_{\text{cyto}} + \frac{\sigma_{\text{cyto}}}{i\omega}$. The volume fraction of the core is the volume fraction occupied by the cytoplasm:

$$\phi_{\text{core}} = \phi_{\text{cyto}} = \frac{a^2 c}{(a+d)^2 (c+d)} \tag{5}$$

d being the membrane thickness.

4 Dividing Cells

Obtaining the equivalent permittivity of dividing cells is more complicated. We provide and compare three approximations: a single-relaxation formula extending the single-cell analysis given above; a double-relaxation formula taking into account the presence of the narrow neck joining mother and daughter cell; and finally, a finite element simulation as an alternative means of obtaining the complex permittivity ϵ_p^*.

Supplementary Fig. 1 compares the three solutions. The single-relaxation formula gives an order of magnitude estimate; however, the model fails to account for the detailed influence of the presence of the neck, and in particular for the low-frequency relaxation due to neck. The finite element simulation clearly indicates the presence of this low-frequency relaxation, in agreement with finite element simulations of dividing yeast cells previously reported in literature[6]. The double-relaxation analytical formula finally agrees well with the results obtained from the finite element simulation.

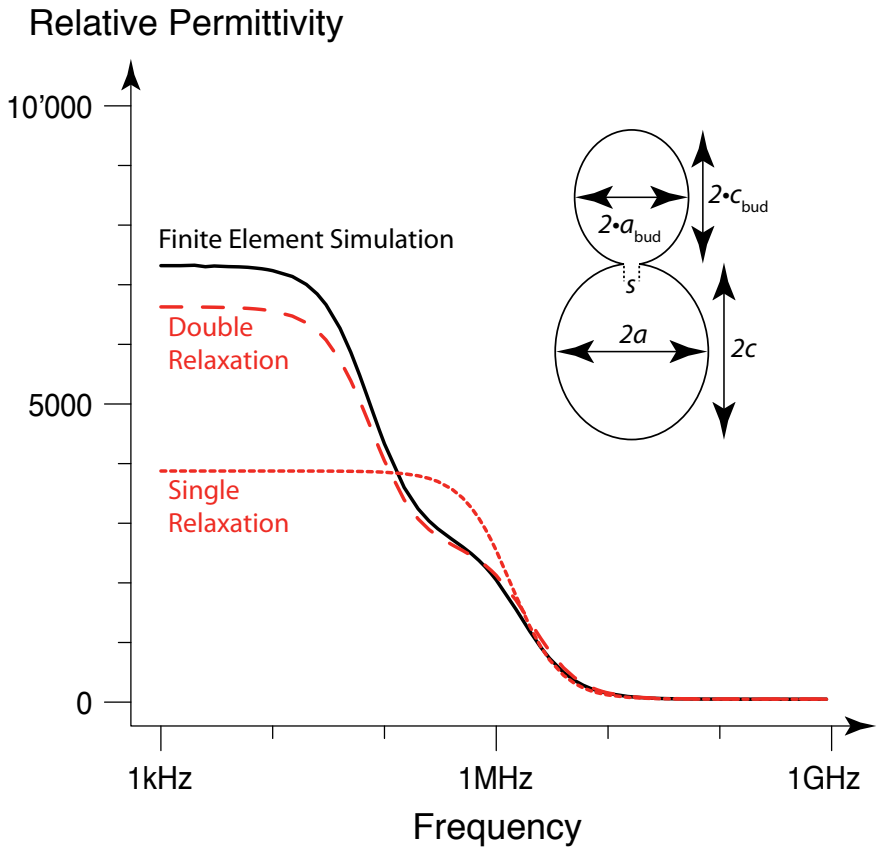

Supplementary Figure 1: Comparison of finite element simulation with the single relaxation and double relaxation analytical solutions in terms of the real part of the equivalent particle permittivity ϵ_p^*. The three approaches are evaluated for a sample yeast geometry, chosen to reflect neck closing during cytokinesis. The half axis values used for the yeast geometry are indicated in the inset, their numerical values are: $a = 3.11\mu$m, $c = 3.58\mu$m, $a_{\text{bud}} = 2.32\mu$m, $c_{\text{bud}} = 2.74\mu$m, for a neck diameter of $s = 311$nm. The single-relaxation model is obtained by evaluating the single-cell model with appropriate volume fractions and form factors as described in section 4.1; the double-relaxation model is described in section 4.2, while the finite element simulation is described in section 4.3. The material constants used are listed in table 1.

4.1 Single Relaxation Formula

A first approximation for the equivalent permittivity of dividing yeast cells can be obtained by applying minor adjustments to the single cell model described above. Indeed, it is straightforward to use eq. 2 with form factors and cytoplasmic volume fractions reflecting the mother-bud geometry. The volume fraction occupied by the cytoplasm for a cell doublet with half axis values a and c for the mother, a_{bud} and c_{bud} for the daughter, membrane thickness d and cytoplasmic neck diameter s can be estimated by:

$$\phi_{\text{core}} = \phi_{\text{cyto}} = \frac{a^2 c \cdot \left[2 - \left(\frac{s}{2a}\right)^3\right] + a_{\text{bud}}^2 c_{\text{bud}} \cdot \left[2 - \left(\frac{s}{2a_{\text{bud}}}\right)^3\right]}{(a+d)^2 (c+d) \cdot \left[2 - \left(\frac{s_{\text{outer}}}{2(a+d)}\right)^3\right] + (a_{\text{bud}}+d)^2 (c_{\text{bud}}+d) \cdot \left[2 - \left(\frac{s_{\text{outer}}}{2(a_{\text{bud}}+d)}\right)^3\right]} \tag{6}$$

where the outer neck diameter s_{outer} is given by:

$$s_{\text{outer}} = 2\sqrt{2d \cdot a_{\text{bud}} + d^2 + \left(\frac{s}{2}\right)^2} \tag{7}$$

Eq. 6 and 7 are obtained by elementary trigonometry and calculus.

An expression for the form factor n_x for yeast doublets is given Supplementary Data 4, equation 19.

Evaluation of the single cell model with adapted form factors and volume fractions allows to obtain correct order of magnitude estimations for the permittivity of dividing yeast cells. This is because adapting the form factor allows to take into account the globally elongated shape of the doublets, whereas the adapted cytoplasmic volume fraction ϕ_{core} as given by eq. 6 allows to take into account the increased relative amount of cell membrane present in the doublets with small daughters as compared to singlets. The single-relaxation formula fails however to account for the low-frequency second dispersion typical for dividing yeast[6].

4.2 Double Relaxation Formula

An analytical approximation to the double-relaxation behaviour of dividing yeast cells observed in numerical simulations[6] can be obtained by considering the physical behaviour of the current flow through a dividing yeast cell. In particular, we consider two current paths through a dividing yeast cell doublet, as shown in Supplementary Fig. 2. The high frequency path avoids the neck, but requires four capacitive passages through cell membranes. It is a relatively low resistivity path, since the neck is avoided, giving rise to its major contribution at high frequency. Its contribution to the total cell permittivity ϵ_p^* is given by ϵ_{hf}^*. The current path through the neck implies higher capacitance, since only two membrane capacitor elements are in series rather than four as for the high frequency path. However, due to the high neck resistivity, the cutoff frequency for this path will be lower. We shall now analyse the high and low frequency contribution in turn.

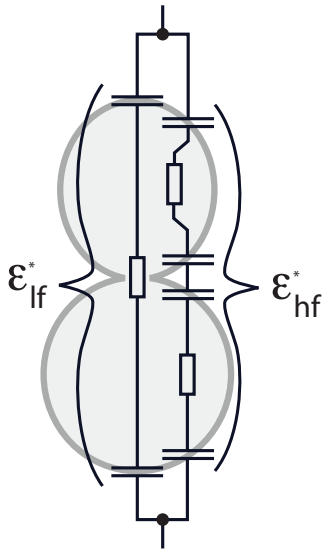

Supplementary Figure 2: Alternative current pathways through a dividing yeast cell. The low-frequency pathway is characterized by a additional capacitance since less membrane elements are in series, but a lower cut-off frequency due to the high resistivity of the cytoplasmic neck in particular during cytokinesis. In terms of complex permittivity, the low-frequency pathway gives rise ϵ^*_{lf}, the high-frequency pathway to ϵ^*_{hf}.

High Frequency Pathway At high frequency (in our experimental settings, above 1MHz), the impedance due to the cell membrane is relatively low as compared to the impedance of the cytoplasm. As a consequence, a substantial voltage drop occurs over the cytoplasm and in particular the neck. This means that mother and daughter cell are to a first approximation polarized as if the were suspended alone in medium. Since the equivalent permittivity of a particle is described by the induced dipole moment per volume, such independent behaviour means that at high frequency, the doublet will have an equivalent permittivity corresponding to a single cell.

In practice, mother and daughter have different size, so their equivalent permittivities are not exactly equal. The question is how to obtain an averaged permittivity, and there are several possibilities leading to only slightly different results, such as volume-weighted averaging of the individual equivalent permittivities, average cell geometry in terms of the half axis radii but single estimation of the equivalent permittivity, estimation of the cell geometry from the total volume divided by two followed by estimation of the permittivity and many more.

We choose the following approach: in order to correctly reflect the total amount of membrane present with respect to cytoplasmic volume, we use the core volume fraction as defined by eq. 6:

$$\phi_{\text{hf}} = \frac{a^2 c \cdot \left[2 - \left(\frac{s}{2a}\right)^3\right] + a_{\text{bud}}^2 c_{\text{bud}} \cdot \left[2 - \left(\frac{s}{2a_{\text{bud}}}\right)^3\right]}{(a+d)^2 (c+d) \cdot \left[2 - \left(\frac{s_{\text{outer}}}{2(a+d)}\right)^3\right] + (a_{\text{bud}}+d)^2 (c_{\text{bud}}+d) \cdot \left[2 - \left(\frac{s_{\text{outer}}}{2(a_{\text{bud}}+d)}\right)^3\right]} \tag{8}$$

where the subscript indicates the use of this volume fraction for the high-frequency part of

the permittivity.

For the cell geometry, we use the mother half axis-radii a and c, since the mother has the bigger volume and therefore contributes more importantly to the equivalent permittivity:

$$n_{x\,,\,\mathrm{hf}} = \frac{1}{1-\left(\frac{c}{a}\right)^2} - \frac{c}{a}\cdot\frac{\ln\left(\frac{c}{a}-\sqrt{\left(\frac{c}{a}\right)^2-1}\right)}{\left[\left(\frac{c}{a}\right)^2-1\right]^{\frac{3}{2}}} \tag{9}$$

Form factor and cytoplasmic volume fraction are sufficient to obtain the high frequency equivalent permittivity[3,4]:

$$\epsilon^*_{\mathrm{hf}} = \epsilon^*_{\mathrm{mem}}\cdot\frac{1+3(1-n_{x\,,\,\mathrm{hf}})\cdot\phi_{\mathrm{hf}}\cdot f_{\mathrm{hf}}}{1-3n_{x\,,\,\mathrm{hf}}\cdot\phi_{\mathrm{hf}}\cdot f_{\mathrm{hf}}} \tag{10}$$

with

$$f_{\mathrm{hf}} = \frac{1}{3}\cdot\frac{\epsilon^*_{\mathrm{cyto}}-\epsilon^*_{\mathrm{mem}}}{\epsilon^*_{\mathrm{mem}}+n_{x\,,\,\mathrm{hf}}\cdot\left(\epsilon^*_{\mathrm{cyto}}-\epsilon^*_{\mathrm{mem}}\right)} \tag{11}$$

Evaluation of eq. 10 along with eq. 8, 9 and 11 determines ϵ^*_{hf}, completing our derivation for the high frequency path.

Low Frequency Pathway At low frequency (for our experimental conditions, less than 20-50kHz) the cell membranes are high-impedance obstacles to the current flow. This implies maximum volt-

age drop across the membranes and hence maximum charge accumulation, leading to the highest equivalent permittivity values. It essentially means that all the membranes fully contribute to the equivalent permittivity of the doublet, and we expect the permittivity at low frequency to be the sum of mother and daughter permittivity rather than some form of average as observed at high frequency.

In terms of the low- and high-frequency pathway scheme outlined in Supplementary Fig. 2, this means that the total permittivity at low frequency should be approximately the sum of mother and daughter equivalent permittivity. Permittivities of parallel pathways are additive, and since the high-frequency pathway represents mainly the mother permittivity, the capacitive part of the low frequency pathway should reflect mainly the permittivity contributed by the daughter membrane capacitance.

We therefore need to obtain the membrane contribution to the permittivity of the daughter cell taken alone. For this, let us apply an imaginary homogeneous electric probe field E over the daughter, and evaluate the resulting dipole moment P, in order to be able to calculate the equivalent permittivity according its primary physical meaning: dipole moment per unit volume per applied field strength. In mathematical terms:

$$\epsilon_{\mathrm{d}}^{*} = \frac{P}{V \cdot E} \tag{12}$$

At low frequency, most of the voltage drops over the membrane, such that the voltage drop

ΔU over the membrane is given by $E \cdot z$, z being the distance from the equator plane of the cell. Considering the membrane to locally behave like a plate capacitor, this leads to a charge density of $\frac{\mathrm{d}Q}{\mathrm{d}A} = E \cdot z \cdot \frac{\epsilon^*_{\mathrm{mem}}}{d}$ accumulated at the membrane. Due to the inclination of the membrane in the ellipsoidal geometry used here, the charge density per unit area projected onto the equator plane is bigger: $\frac{\mathrm{d}Q}{\mathrm{d}A_{\mathrm{equator}}} = E \cdot c_{\mathrm{bud}} \cdot \frac{\epsilon^*_{\mathrm{mem}}}{d}$. For the calculation of the equivalent permittivity, we exclusively need to take into account the charges accumulating at the outer membrane surface, such that the dipole moment per unit area becomes: $\frac{\mathrm{d}P}{\mathrm{d}A_{\mathrm{equator}}} = 2z \cdot E c_{\mathrm{bud}} \cdot \frac{\epsilon^*_{\mathrm{mem}}}{d}$. Since the volume of the cell arising per unit area of the equator plane is given by $\mathrm{d}V = 2z \cdot \mathrm{d}A_{\mathrm{equator}}$, we conclude that the external dipole moment per unit volume is constant and given by $\frac{\mathrm{d}P}{\mathrm{d}V} = E \cdot \epsilon^*_{\mathrm{mem}} \cdot \frac{c_{\mathrm{bud}}}{d}$. Therefore, the daughter membrane contribution to the permittivity follows:

$$\epsilon^*_{\mathrm{d}} = \epsilon^*_{\mathrm{mem}} \cdot \frac{c_{\mathrm{bud}}}{d} \tag{13}$$

It remains to estimate the series contribution of the neck, as illustrated by the resistive element in the low-frequency pathway in Figure 2. Again, we make use of the fundamental link between induced dipole moment and equivalent permittivity to estimate the contribution of the neck to the permittivity:

$$\epsilon^*_{\mathrm{neck}} = \frac{P}{V \cdot E} \tag{14}$$

We model the neck as a disk joining mother and daughter cell. For the relatively small neck

sizes typical for yeast cells, to a first approximation, we can consider the capacitance between the neck disk and an infinitely big counter electrode infinitely far away from the neck to calculate the charge that will be accumulated at the neck, the space between disk and counter electrode being filled with cytoplasm. The capacitance of a disk of radius $r = \frac{s}{2}$ to an infinite electrode is given by $C^* = \epsilon^*_{\text{cyto}} \cdot 8r$; since we consider only the daughter, we need to take into account half of this capacitance, so that we finally have:

$$C^*_{\text{neck}} = \epsilon^*_{\text{cyto}} \cdot 4r \tag{15}$$

In reality, the counter electrode is neither infinitely big nor infinitely far way, but corresponds to the membrane surrounding the rest of the daughter cell. Hence, for calculation purposes, the counter charge can be lumped together at the center of the daughter cell, such that when applying a probe field of strength E, we get a voltage of $U = E \cdot c_{\text{bud}}$ over the neck capacitance C^*_{neck} and hence a total charge of $Q_{\text{neck}} = \epsilon^*_{\text{cyto}} \cdot 4r \cdot c_{\text{bud}} E$. For small neck sizes c_{bud} also approximately corresponds to the distance between the neck disk and the center of the daughter cell, so the dipole moment is given by $P \approx Q_{\text{neck}} c_{\text{bud}} = \epsilon^*_{\text{cyto}} \cdot 4r \cdot c^2_{\text{bud}} E$. Applying eq 14 and $V = \frac{4\pi}{3} c_{\text{bud}} a^2_{\text{bud}}$, we get for the neck equivalent permittivity:

$$\epsilon^*_{\text{neck}} = \epsilon^*_{\text{cyto}} \cdot \frac{3}{\pi} \cdot \frac{r \cdot c_{\text{bud}}}{a^2_{\text{bud}}} \tag{16}$$

The permittivity elements ϵ^*_{neck} and ϵ^*_{d} in series define the total equivalent permittivity of the

low-frequency pathway in Figure 2. Permittivities in series add up as would resistors in parallel, such that we have for the low-frequency pathway:

$$\epsilon^*_{\mathrm{lf}} = \frac{\epsilon^*_{\mathrm{neck}} \cdot \epsilon^*_{\mathrm{d}}}{\epsilon^*_{\mathrm{neck}} + \epsilon^*_{\mathrm{d}}} \tag{17}$$

Equivalent Permittivity of Dividing Yeast Cells For the equivalent permittivity of the dividing yeast, we need to add up the parallel permittivities of the high and low-frequency pathways. We therefore have:

$$\epsilon^*_p = \epsilon^*_{\mathrm{lf}} + \epsilon^*_{\mathrm{hf}} \tag{18}$$

where ϵ^*_{lf} is given by eq. 17 and ϵ^*_{hf} by eq. 10. Especially for small neck sizes, ϵ^*_{lf} shows a lower relaxation frequency than ϵ^*_{hf}, giving rise to a double interfacial relaxation across the kHz to MHz range.

Supplementary Fig. 1 finally compares the single- and double-relaxation solutions to a finite element estimation of the complex permittivity of a given dividing yeast doublet obtained with the commercial software COMSOL. It is seen that the single-relaxation formula correctly predicts the high frequency part, and gives an order of magnitude estimation at low frequencies. Not surprisingly, the match between the double-relaxation formula and finite element simulation is better. The details of the finite element simulation are to be given below.

4.3 Finite Element Simulation

We use the commercial software COMSOL for the finite element simulations. Most of the work for obtaining a simulation consists in drawing and assigning the correct material properties and physical equations to the different domains and boundaries, according to the manufacturer's instructions. There are however two noteworthy exceptions: Firstly, it is difficult to obtain correct meshing in the presence of the cell membrane, the thickness of which is orders of magnitude smaller than the typical dimensions of the yeast cells; and secondly, we need a strategy to obtain the equivalent permittivity from a quantity directly accessible in COMSOL.

We address the first point by not drawing the cell membrane as its own spatial region, but rather by imposing a particular boundary condition between cytoplasm and extracellular medium. This boundary condition links cross-membrane current density to the membrane conductivity and permittivity, according to:

$$j_{\text{cross-membrane}} = [\sigma_{\text{mem}} + j\omega \cdot \epsilon_{\text{mem}}] \cdot \frac{\Delta V}{d} \tag{19}$$

In order to obtain the equivalent permittivity of the dividing yeast by finite element simulation in COMSOL we match the impedance observed for the cell as modelled by cytoplasm and membrane regions, and second, for a particle of identical geometry but homogeneous composition. Indeed, the complex permittivity that gives rise to the same impedance as the one obtained for the cell composed of membrane and cytoplasm is by definition the equivalent complex permittivity ϵ_p^*

we are looking for.

1. Asami, K., Hanai, T. & Koizumi, N. Dielectric properties of yeast cells. *Journal of Membrane Biology* **28**, 169–180–180 (1976-12-01).

2. Huang, Y., Holzel, R., Pethig, R. & Wang, X. Differences in the ac electrodynamics of viable and nonviable yeast-cells determined through combined dielectrophoresis and electrorotation studies. *Physics In Medicine And Biology* **37**, 1499 (1992).

3. Castellarnau, M., Errachid, A., Madrid, C., Juarez, A. & Samitier, J. Dielectrophoresis as a tool to characterize and differentiate isogenic mutants of escherichia coli. *Biophysical Journal* **91**, 3937–3945 (2006).

4. Huang, J. P., Yu, K. W., Lei, J. & Sun, H. Spectral representation theory for dielectric behavior of nonspherical cell suspensions. *Communications In Theoretical Physics* **38**, 113–120 (2002).

5. Sihvola, A. *Electromagnetic mixing formulas and applications* (The Institution of Electrical Engineers, 1999).

6. Asami, K. & Sekine, K. Dielectric modelling of cell division for budding and fission yeast. *Journal Of Physics D-Applied Physics* **40**, 1128–1133 (2007).

Supplementary information 4: Form Factor for the yeast cells

This supplementary information explains how to obtain the form factors, needed for the evaluation of the Clausius-Mossotti factors and hence the dielectrophoretic force.

1 Problem Statement

From an electrical point of view, the yeast cells in the culture medium are dielectric inclusions in a homogeneous dielectric. Such inclusions are polarized under the influence of an external electric field; the resulting polarization of the inclusions is however not just dependent on the external field, but actually the result of the interaction between the primary external field and secondary fields resulting from particle polarization. As a result, the polarization of dielectric inclusions will be in equilibrium with the total field composed of external and induced field, rather than just the external field as one might expect naively. This is the basis of the Clausius-Mossotti theory. Indeed, the Clausius-Mossotti factor, which determines the magnitude and sign of the dielectrophoretic force, depends explicitly on the form factor n_x:

$$f_{\mathrm{CM}}(\omega) = \frac{\epsilon_p^*(\omega) - \epsilon_m^*(\omega)}{\epsilon_m^*(\omega) + \left[\epsilon_p^*(\omega) - \epsilon_m^*(\omega)\right] \cdot n_x} \tag{1}$$

In terms of the physics involved, the form factor, also referred to as Lorentz depolarization factor, describes the strength of the secondary field relative to what would be observed in an ideal

plate condenser with an identical electric polarization P and dielectric constant ϵ. The task in this supplementary information is to obtain an expression for the form factor n_x of single and, most importantly, dividing yeast cells.

2 Basic Physics

In general, the polarization P gives rise to surface charges, and these surface charges in turn give rise to the secondary electric field. In an ideal plate condenser, the surface charge is related to the polarization P by:

$$\frac{Q}{A} = P \tag{2}$$

The magnitude of the secondary electric field, in turn, is given by

$$E_{\text{secondary}} = -\frac{Q}{A \cdot \epsilon} = -\frac{P}{\epsilon} \tag{3}$$

For dielectric inclusions in general, the magnitude of the secondary field will be less than $\left|\frac{P}{\epsilon}\right|$, and the form factor n_x indicates the relation between the polarization P and the resulting secondary field:

$$n_x = -\frac{E_{\text{secondary}} \cdot \epsilon}{P} \tag{4}$$

the minus sign indicating that in general the secondary field vector will be opposed to the polarization, whereas the form factor is positive.

3 Single Cells

We model single yeast cells by spheres or prolate ellipsoids with rotational symmetry, according to the their growth stage (see supplementary information 2).

For a dielectric sphere, the internal field is given by $E_{\text{secondary}} = -\frac{P}{3\epsilon}$ such that the form factor is given by[1] $n_x = \frac{1}{3}$. For ellipsoidal inclusions with cylindrical symmetry (that is with half axes $a = b$, but generally different c) the form factor is given by[1]:

$$n_x = \frac{1}{1 - \left(\frac{c}{a}\right)^2} - \frac{c}{a} \cdot \frac{\ln\left(\frac{c}{a} - \sqrt{\left(\frac{c}{a}\right)^2 - 1}\right)}{\left[\left(\frac{c}{a}\right)^2 - 1\right]^{\frac{3}{2}}} \tag{5}$$

where the electric field vector is along c. We use this expression for the form factor of the non-dividing yeast cells.

4 Dividing Cells

We model the dividing yeast cells by joined ellipsoids, with a common cylindrical symmetry axis. This means that both the mother and the daughter cell are represented by a rotationally symmetric ellipsoid that is cut open by the neck plane. In order to calculate the form factor, we shall first

estimate the strength of the secondary electric field, by calculating the surface charges and then applying Coulomb's law.

For an arbitrarily shaped dielectric body with constant polarization P, the surface charge is given by:

$$\mathrm{d}Q = \overrightarrow{P} \cdot \mathrm{d}\overrightarrow{A} = P\mathrm{d}A \cdot \cos\gamma \tag{6}$$

where γ is the angle between the polarization vector and the surface element.

We shall now first consider the electric field of an ellipsoid that is cut open. We parameterize the ellipsoid using the planetary angle, such that $x = a\cos\alpha$ and $y = c\sin\alpha$, the rotational symmetry axis being along y.

For a rotationally symmetric ellipsoid, the surface charge on a ring of constant latitude α can be estimated from:

$$\mathrm{d}Q = P \cdot 2\pi a^2 \sin\alpha\cos\alpha \cdot \mathrm{d}\alpha \tag{7}$$

The electric field due to this charge ring, on an arbitrary position $y = d$ along the symmetry axis is obtained by Coulomb's law and the realization that only the component along the symmetry axis subsists, the perpendicular component nulling out due to the cylindrical symmetry, giving rise

to elementary trigonometric considerations:

$$\mathrm{d}E = \frac{\mathrm{d}Q \cdot (d - c\sin\alpha)}{4\pi\epsilon \cdot \left[a^2\cos^2\alpha + (d - c\sin\alpha)^2\right]^{\frac{3}{2}}} \tag{8}$$

Plugging in the expression for the surface charge (eq. 7) we obtain:

$$\mathrm{d}E = \frac{P\sin\alpha\cos\alpha \cdot \mathrm{d}\alpha \cdot \left(\frac{d}{a} - \frac{c}{a}\sin\alpha\right)}{2\epsilon \cdot \left[\cos^2\alpha + \left(\frac{d}{a} - \frac{c}{a}\sin\alpha\right)^2\right]^{\frac{3}{2}}} \tag{9}$$

For a fully close ellipsoid the field is known to be homogeneous within the ellipsoidSihvola1999, such that we can set $d = 0$, and the form factor is obtained by:

$$\begin{aligned} n_x &= -\frac{\epsilon}{P}\int_{-\frac{\pi}{2}}^{\frac{\pi}{2}} \mathrm{d}E = \int_{-\frac{\pi}{2}}^{\frac{\pi}{2}} \frac{\sin^2\alpha\cos\alpha \cdot \mathrm{d}\alpha \cdot \frac{c}{a}}{2 \cdot [1 + [\left(\frac{c}{a}\right)^2 - 1]\sin^2\alpha]^{\frac{3}{2}}} \\ &= \frac{1}{1 - \left(\frac{c}{a}\right)^2} - \frac{c}{a} \cdot \frac{\ln\left(\frac{c}{a} - \sqrt{\left(\frac{c}{a}\right)^2 - 1}\right)}{\left[\left(\frac{c}{a}\right)^2 - 1\right]^{\frac{3}{2}}} \end{aligned} \tag{10}$$

which is the well-known form factor for rotationally symmetric ellipsoids (eq. 5).

For a cut-open ellipsoid two things change. First, we do no more expect the field to be constant over the ellipsoid, such that we need to take into account the position d. And second, we need to adapt the integration boundaries such as to respect the cut.

We characterize the cut plane by the planetary opening angle α_0, such that $y_{\text{CUT}} = c \sin \alpha_0$. To obtain the form factor as it would be estimated by considering the field at a position given by $y = d$, we need to integrate between α_0 and $\frac{\pi}{2}$:

$$E\left(\alpha_0\,,\,d\right) = \frac{P}{\epsilon} \int_{\alpha_0}^{\frac{\pi}{2}} \frac{\sin\alpha\cos\alpha \cdot \mathrm{d}\alpha \cdot \left(\frac{d}{a} - \frac{c}{a}\sin\alpha\right)}{2 \cdot \left[\cos^2\alpha + \left(\frac{d}{a} - \frac{c}{a}\sin\alpha\right)^2\right]^{\frac{3}{2}}} \cdot \mathrm{d}\alpha \tag{11}$$

We define the solution using an indefinite integral, with an arbitrary integration constant C

$$\begin{aligned} f\left(\alpha\,,\,d\right) &= -\int \frac{\sin\alpha\cos\alpha \cdot \mathrm{d}\alpha \cdot \left(\frac{d}{a} - \frac{c}{a}\sin\alpha\right)}{2 \cdot \left[\cos^2\alpha + \left(\frac{d}{a} - \frac{c}{a}\sin\alpha\right)^2\right]^{\frac{3}{2}}} \cdot \mathrm{d}\alpha \\ &= \frac{1}{2 \cdot (c^2 - a^2)} \cdot \left[\frac{a^2 \cdot c \cdot z}{(c^2 - a^2)^{\frac{1}{2}}} - \frac{a}{w} \cdot \left(c \cdot \sin\alpha - d + \frac{cd \cdot (c - d \cdot \sin\alpha)}{(c^2 - a^2 - d^2)}\right)\right] + C \end{aligned} \tag{12}$$

where w is defined as:

$$w\left(\alpha\,,\,d\right) = \left[\cos^2\alpha + \left(\frac{c}{a} \cdot \sin\alpha - \frac{d}{a}\right)^2\right]^{\frac{1}{2}} \tag{13}$$

and z is defined as:

$$z\left(\alpha\,,\,d\right)=\ln\left[\frac{\left(c^2-a^2\right)\sin\alpha-cd}{a^2\sqrt{\left(\frac{c}{a}\right)^2-1}}+w\left(\alpha\,,\,d\right)\right] \tag{14}$$

For the electric field along the axis of the cut-open ellipsoid, we therefore have:

$$E\left(\alpha_0\,,\,d\right)=\frac{P}{\epsilon}\cdot\left[f\left(\alpha_0\,,\,d\right)-f\left(\frac{\pi}{2}\,,\,d\right)\right] \tag{15}$$

The total secondary electric field for a dividing cell is obtained by adding the field from the mother and from the daughter. Compared to the mother, the daughter's cut surface is rotated by 180 degrees; but since relative to the cut surface, this also implies that the polarization vector is inverted, we finally can add the fields directly according to:

$$E_{\text{tot}}\left(d\right)=E_{\text{mother}}\left(\alpha_{0,\text{mother}}\,,\,d\right)+E_{\text{daughter}}\left(\alpha_{0,\text{daughter}}\,,\,-d-s\right) \tag{16}$$

where $s=\left|\sin\alpha_{0,\text{daughter}}\cdot c_{\text{daughter}}\right|+\left|\sin\alpha_{0,\text{mother}}\cdot c_{\text{mother}}\right|$ is the separation between the centres of the mother and daughter ellipsoid, and where E_{mother} and E_{daughter} need to be calculated with the appropriate half axes values a_{mother}, c_{mother} and a_{daughter}, c_{daughter} respectively.

The cut angle values $\alpha_{0,\text{mother}}$ and $\alpha_{0,\text{daughter}}$ can be calculated from the neck radius r_n via:

$$r_n=a_{\text{mother}}\cdot\cos\alpha_{0,\text{mother}}=a_{\text{daughter}}\cdot\cos\alpha_{0,\text{daughter}} \tag{17}$$

taking the solution in the interval $[0, -\frac{\pi}{2}]$.

The electric field is not constant over the cell pair, so we take the volume weighted average as measure of the mean electric field due to the polarization P:

$$< E >= \frac{\int A(d) \cdot E_{\text{tot}}(d) \cdot \mathrm{d}d}{V_{\text{tot}}} \tag{18}$$

$$\begin{aligned} n_x &= -\frac{\epsilon \cdot < E >}{P} \\ &= \frac{\int A(d) \cdot \left[f_m\left(\frac{\pi}{2}\,, d\right) + f_d\left(\frac{\pi}{2}\,, d\right) - f_m\left(\alpha_{0,\text{mother}}\,, d\right) - f_d\left(\alpha_{0,\text{daughter}}\,, -d-s\right) \right] \mathrm{d}d}{V_{\text{tot}}} \end{aligned} \tag{19}$$

where the subscripted symbols f_m and f_d indicate the f as defined by eq. 12 should be evaluated with suitable half axis values corresponding to the mother and daughter geometry.

We carry out this last integration step numerically.

1. Sihvola, A. *Electromagnetic mixing formulas and applications* (The Institution of Electrical Engineers, 1999).